Correlation between power harrow energy demand and tilled soil aggregate dimensions

CORRELATION BETWEEN POWER HARROW ENERGY DEMAND AND TILLED SOIL AGGREGATE DIMENSIONS

Massimiliano Varani[a], *Michele Mattetti*[a*], *Giovanni Molari*[a]
Alessandro Biglia[b], *Lorenzo Comba*[b],

[a] Department of Agricultural and Food Sciences – Alma Mater Sudiorum - University of Bologna, viale G. Fanin 50, Bologna, Italy
[b] Department of Agricultural, Forest and Food Sciences (DiSAFA) – Università degli Studi di Torino, Largo Paolo Braccini 2, 10095 Grugliasco (TO), Italy
[*] Michele Mattetti, tel. +39 051 2096174, fax +39 051 2096178, e-mail: michele.mattetti@unibo.it

Abstract

Energy demand of soil tillage implements has been reported based on different operating conditions and the chemical and physical soil properties. However, tillage operations cannot only be evaluated according to their energy consumption; the soil structure improvement and the consequent agronomic benefits must also be considered. Power harrows can adjust soil clod size by varying the velocity ratio (λ) of the machinery which is calculated from the ratio of the peripheral speed of the tine rotors and the vehicle's advancing speed. This paper aims to gain deeper insight into controlling the soil structure and find correlations with the power harrow's energy requirement in different setups. Field tests were conducted at the experimental farm of the University of Bologna on a 3-m working width power harrow coupled with a tractor with 107 kW of rated engine power. Field tests were performed by varying λ from 1.46 to 7.90 while tractor parameters, such as speed, engine power, fuel rate consumption, draught, and power take-off (PTO) speed and torque, were acquired with a datalogger. After harrowing, soil samples were sieved and significant granulometric parameters were calculated and correlated to data acquired from the tractor–power harrow system. The results show that the optimum conditions for a high-quality seedbed are obtained with high values of implement–soil impact speed, whilst λ should be kept as low as possible to minimise the fuel consumption per ha.

KEYWORDS: CO_2 emissions; soil loosening; seedbed preparation; tillage; energy

Nomenclature		
β	Tractor engaged gear	(-)
δ	Implement working depth	(mm)
λ	Velocity ratio	(-)
τ_{ph}	Power harrow transmission ratio	(-)
τ_{PTO}	Tractor power take-off (PTO) transmission ratios	(-)
η	Power delivery efficiency	(-)
b	Power harrow working width	(m)
d_i	Dimension of the holes in the i^{th} sieve	(mm)
$\dot{f}$	Fuel consumed by the tractor engine per unit of time	(l h^{-1})
f_{ha}	Fuel consumption per hectare	(l ha^{-1})
n_e	Revolution speed of the tractor engine crankshaft	(rev min^{-1})
n_{ph}	Revolution speed of the power harrow tines	(rev min^{-1})
n_{PTO}	Revolution speed of the tractor PTO	(rev min^{-1})
k_s	Index of soil skeleton	(-)
k_t	Index of soil texture	(-)
D	Draught force between the tractor and the power harrow	(kN)
E	Energy required to process 1 m^3 of tilled soil	(kJ m^{-3})
F_c	Field capacity	(ha h^{-1})
GMD	Geometric mean diameter of soil aggregates	(mm)
M_e	Tractor torque as a percentage of M_r	(%)
M_f	Tractor sum of the engine frictional and thermodynamic loss, pumping torque loss, and losses of fuel, oil, and cooling pumps as a percentage of M_r	(%)
M_{ph}	Torque applied to the power harrow rotors	(Nm)
M_r	Maximum tractor engine torque available	(Nm)
M_{PTO}	Torque delivered at the tractor PTO	(Nm)
MWD	Mean weight diameter of soil aggregates	(mm)
P_e	Actual tractor engine power	(kW)
P_D	Draught power between the tractor and the power harrow	(kW)
P_{ph}	Power absorbed by the power harrow	(kW)
P_{PTO}	Power required to run the power harrow rotors through the PTO	(kW)
R_{ph}	Radius of power harrow rotors	(m)
V_{is}	Maximum implement–soil impact speed	(km h^{-1})
V_t	Tractor ground speed	(km h^{-1})
$W_{i,j}^{r\%}$	Percentage of soil mass retained in the i^{th} sieve from a sample collected in the j^{th} parcel	(%)
$W_{j,0-8}$	Mass of soil with clods between 0 and 8 mm	(kg)
$W_{j,>8}$	Mass of soil with clods over 8 mm	(kg)
$W_{j,>32}$	Mass of soil with clods over 32 mm	(kg)

1. Introduction

Population growth requires increased global food production, which should not occur at the expense of greenhouse gas (GHG) emissions mitigation (Beckman et al., 2020). Researchers and policy-makers have been working to find solutions that will support the sustainable intensification of modern farming systems to increase their productivity while minimising their

environmental footprint (Garnett et al., 2013). In 2020, the European Commission (EC) presented strategies to achieve this goal including “Farm-to-Fork”, “Biodiversity Strategies”, and the “European Green Deal”. Within these strategies, one area of improvement is sustainable food production, which should be based on agricultural practices that can reduce GHG emissions, inputs (e.g., water, fertilisers, and chemical pesticides), and direct energy consumption (Balázs et al., 2021).

Among agricultural operations, tillage is the most energy-intensive operation in primary production. Tillage accounts for about one-quarter of the total energy input for crop production (Borin et al., 1997), and currently 92% of this energy is supplied by fossil fuels (Choudhary et al., 2021). Several studies have thoroughly characterised the energy demand of the tractor–implement system under different operating conditions (i.e., working depth and speed) (Balsari et al., 2021; Godwin et al., 2007; Mattetti et al., 2017), and different soil types and moisture levels (Natsis et al., 1999). However, tillage operations cannot only be evaluated by their energy demand; the benefits for soil structure and other agronomic aspects (e.g., crop yield) must also be considered.

Tillage modifies soil structure via mechanised implements. It requires substantial energy to cut soil, invert soil layers, reduce clod size, and rearrange aggregates. Soil structure is defined as the size, shape, and arrangement of soil particles and pores; it is crucial for germination and crop growth and to regulate soil water content (Adam & Erbach, 1992; Bronick & Lal, 2005). Typically, finer soil aggregates result in higher field emergence and crop yield (Heege, 2013); however, excessive tillage is undesirable as it contributes to increased soil vulnerability to wind and water erosion (Tapela & Colvin, 2002). It is generally accepted that an aggregate size of 1 to 8 mm is required for a good seedbed (Adam & Erbach, 1992; Braunack & Dexter, 1989; Munkholm, 2002; Tapela & Colvin, 2002), but deviations from this general rule should be adopted according to the crop, weather, rainfall, and type of soil. For example, in Europe spring

barley needs finer soil aggregates than winter wheat as it is usually sown in drier periods (USDA, 1984). Soils with a high clay content can accept a coarser soil structure due to their swelling–shrinking ability, which permits the soil particles to disintegrate (Heege, 2013). Soil structures are usually evaluated via indicators, the most popular of which are the mean weight diameter (MWD) and the geometric mean diameter (GMD) (Daraghmeh et al., 2019; Natsis et al., 1999; Nunes et al., 2015; Van Bavel, 1950; Weill et al., 1989).

To obtain the desired size of soil aggregates in the topsoil using conventional tillage management, secondary tillage operations are conducted. In Europe, the power harrow is a widely adopted machinery for secondary tillage because it produces a viable seedbed and it requires only limited tractor draught, ensuring minimal losses due to wheel-slip and rolling resistance. (Chen et al., 2005; Scarlett, 2001). Moreover, unlike other power take-off (PTO)-driven tillage machinery, such as the rotary tiller, power harrows do not create tillage hardpan (Sukcharoenvipharat & Usaborisut, 2018). Soil clod size can be adjusted with power harrows through the machinery ground speed and the angular speed of tine rotors as both control the number of tine revolutions per metre moved (Celik & Altikat, 2022; Raparelli et al., 2020). This may also affect the energy required for operation; Balsari et al. (2021) found that the specific energy (i.e., the energy per unit area or volume) may increase by up to 40% when the rotating speed of the tines is increased while the machine ground speed is kept constant. Conversely, as with rotary tillers (Daraghmeh et al., 2019; Watts et al., 1996), increasing the ground speed should reduce the specific energy without changing the rotating speed of the tines due to the increased field capacity. Upadhyay & Raheman (2020a, 2020b) investigated the impact of velocity ratio for a different type of PTO-driven implement, and discovered that, up to a certain point, the specific energy requirement decreased with an increase in velocity ratio, and then increased with further increases in velocity ratio.

Studies investigating the optimal operating parameters of power harrows in terms of the energy used and the soil structure are lacking.

This paper aims to gain deeper insights into controlling the soil structure and find a correlation between the energy requirements of the machinery and the subsequent soil structure using different power harrow setups.

2. Materials and methods

2.1. Tractor and power harrow

The tests were performed with a 3-m working width (b) power harrow (Frandent Eternum R303-19, Frandent Group Srl, Italy) equipped with a packer roller. The selected power harrow was equipped with a gearbox used to change the transmission ratio (τ_{ph}) between the PTO and the tine rotors. The specifications of the power harrow are reported in Table 1 while its photo is reported in Figure 1a.

Table 1. Power harrow specifications

Parameter	Value
Working width (b) [m]	3
Number of rotors	12
Rotor radius (R_{ph}) [m]	0.1
Rotor tine length [mm]	290
Roller diameter [mm]	550
Mass (harrow + roller) [kg]	1,323

This model of power harrow was chosen for the study because its main specifications are very common on the Italian market. The power harrow was pulled by a four-wheel-drive row crop tractor; Table 2 presents the tractor specifications.

107 **Table 2.** Tractor specifications and PTO transmission ratios

Parameter	Value	
Manufacturer	CNH Industrial N.V. (Amsterdam, Netherlands)	
Model	Case IH Maxxum 115	
Unladen mass [kg]	4,890	
Rated engine speed [rpm]	2,000	
Maximum engine power at rated engine speed [kW]	107	
Transmission	Partial-powershift, 16 forward and 16 reverse speeds	
PTO transmission ratios in different modes (τ_{PTO})	540 mode	0.27
	540E mode	0.35
	1000 mode	0.50

108

109 *2.2. Sensors and acquisition system*

110 The tractor parameters were acquired through the tractor's controller area network (CAN) SAE
111 J1939 diagnostic port and recorded with a Kvaser Memorator 2 datalogger (Kvaser Inc.,
112 Mission Viejo, CA, USA) using the following suspect parameter numbers (SPNs) and
113 parameter group numbers (PGNs):

114 • SPN 544 and PGN 65251: '*Engine Reference Torque*' reports the maximum engine
115 torque available (M_r) at a sampling rate of 0.2 Hz.

116 • SPN 513 and PGN 61444: '*Actual Engine – Per cent Torque*' reports the torque (M_e)
117 as a percentage of M_r at a sampling rate of 50 Hz.

118 • SPN 513 and PGN 5398: '*Nominal Friction – Per cent Torque*', denoted as M_f,
119 reports the sum of the engine frictional and thermodynamic loss, pumping torque
120 loss, and losses of fuel, oil, and cooling pumps as a percentage of M_r at a sampling
121 rate of 20 Hz.

122 • SPN 190 and PGN 61444: '*Engine Speed*' reports the revolution speed of the engine
123 crankshaft (n_e) at a sampling rate of 10 Hz.

- SPN 523 and PGN 61445: '*Transmission Current Gear*' reports the engaged gear in the tractor transmission (β) at a sampling rate of 10 Hz.
- SPN 1883 and PGN 65090: '*Rear PTO Output Shaft Speed*' reports the speed of the rear PTO (n_{PTO}) at a sampling rate of 10 Hz.
- SPN 183 and PGN 65266: '*Engine Fuel Rate*' reports the fuel consumed by the engine per unit of time ($\dot{f}$) at a sampling rate of 10 Hz.
- SPN 1873 and PGN 65093: '*Rear Hitch Position*' reports the position of the rear three-point hitch at a sampling rate of 10 Hz.
- SPN 8768 and PGN 8960, '*Hitch Information – Rear in Work*' reports the status of the rear three-point linkage (TPH), which is equivalent to 1 when the TPH is in working position and 0 when the TPH is lifted. It is denoted as H_{tph} and measured at a sampling rate of 10 Hz.

The ground speed of the tractor (V_t) and its geolocation were measured using a global navigation satellite system (GNSS) receiver (IPEspeed, Ipetronik GmbH & Co. KG, Baden-Baden, Germany) with a 10 Hz sampling rate and a circular error probable (CEP) of 2.5 m. The output signal of the GNSS receiver was in the CAN bus protocol, so it was directly connected to the datalogger to record V_t during the tests.

A three-point hitch coupler equipped with three biaxial load pins placed at the hitch points of the three-point linkage was installed between the tractor and the power harrow to measure the draught force (D) (Balsari et al., 2021; Mattetti et al., 2017). The biaxial load pins (N.B.C. Elettronica Group Srl, Italy) were able to take forces along two orthogonal axes with a load capacity of 10 kN in each direction. The pins were installed to record the positive direction of the longitudinal force when the tractor pulled the implement, while the positive direction of the vertical force was aligned with the force of gravity. The torque delivered at the tractor PTO

(M_{PTO}) was measured with a torque meter (NTCE 7000 series, NTCE AG, Germany) with a full scale of 5000 Nm (Fig. 1).

a b

Fig. 1. Photos of the power harrow Frandent Eternum R303-19 (a) and the three-point hitch coupler equipped with load pins and the torque meter used during the tests (b).

As the signals from the load pins and the torque meter were in voltage output and the Kvaser datalogger is only compliant with the CAN bus protocol, a conversion module was used to translate their outputs from analogue to the CAN bus protocol (ADMM 8 pro, CSM Gmbh, Filderstadt, Germany).

2.3. Experimental sites and soil characteristics

Tests were conducted in autumn 2021 at the experimental farm of the University of Bologna located in Cadriano (latitude 44°33'27.6624" and longitude 11°24'35.3844", Emilia Romagna Region, north-central Italy). The climate is classified as humid subtropical (Cfa) according to the Köppen-Geiger climate classification (Köppen, 1936) and is characterised by hot summers and two main rainy periods in spring and autumn. The field used for the test was 200 m long and 50 m wide, and it was classified as silty clay loam soil according to the USDA textural soil

classification (USDA, 1987). This category of soil was chosen since it is considered appropriate for planting very popular crops such as maize or sorghum in north-central Italy. Moreover, the field was completely ploughed at a depth of 250 mm before the test to bury the crop residue. The liquid limit (LL) and the plastic limit (PL) of the soil were 31% and 21%, respectively. A plasticity index (PI) of 10% permitted the soil to be classified as low-plasticity clay (ASTM, 2010). The mean value and the standard deviation of soil bulk density over the field were 1,620 kg m^{-3} and 230 kg m^{-3}, respectively; while the mean value and the standard deviation of the soil moisture content (based on the dry mass) were 20.7% and 1.6%, respectively (ASTM, 2009b). Under these conditions, the soil moisture content was close to the optimum for soil workability (Dedousis & Bartzanas, 2010; Dexter & Bird, 2000).

2.4. Test conditions and experimental design

The rotating speed of the tines (n_{ph}) was calculated as a function of the rear PTO output shaft speed and the gearbox transmission ratio using Eq. (1);

$$n_{ph} = n_{PTO}\ \tau_{ph} \tag{1}$$

The combined effect of V_t and n_{ph} on the tractor performance and soil granulometry was evaluated with the introduction of the velocity ratio (λ) (Hann & Giessibl, 1998; Shinners et al., 1993; Upadhyay & Raheman, 2020a, 2020b) as shown in Eq.(2);

$$\lambda = \frac{n_{ph} R_{ph}}{V_t} \tag{2}$$

where the numerator of the ratio indicates the peripheral speed of the power harrow rotors. Field tests consisted of six unique field operation configurations performed with varying λ from a feasible minimum of 1.46 to a maximum of 7.90, as shown in Table 3. These boundary values were fixed by the physical characteristics of the tractor and the power harrow used for the tests; lower or higher values were too difficult to achieve. As particular λ values can be obtained with

multiple combinations of n_{ph} and V_t, these parameters were selected according to the results of a preliminary field test. The chosen configurations were the best matches to the constraints of the soil characteristics, tractor transmission ratios, and maximum engine power.

Table 3. Trial target configurations

Trial name	n_e [rpm]	V_t [km h^{-1}]	PTO mode	τ_{ph}	n_{ph} [rpm]	λ
T1	2,000	6.6	540E	1.24	256	1.46
T2	2,000	6.6	540E	0.81	398	2.27
T3	2,000	4.0	540E	1.24	256	2.41
T4	2,000	2.5	540	1.24	184	2.77
T5	2,000	3.8	1,000	1.24	340	3.37
T6	2,000	2.1	1,000	0.97	440	7.90

Trials T2, T3, and T4 were designed for λ values of about 2.5 obtained with different combinations of n_{ph} and V_t. The choice to perform multiple trials at about the same λ value was suggested by the power harrow user manual, which indicates 2.5 as the optimal working point to avoid overstressing the rotor bearings.

The field described in section 2.3 was divided into 24 parcels, 4 m in width and 100 m in length as four replicates per configuration were performed (T1-T6). The repetitions were randomised across the field to limit the results' dependence on variations in soil characteristics (Fig. 2).

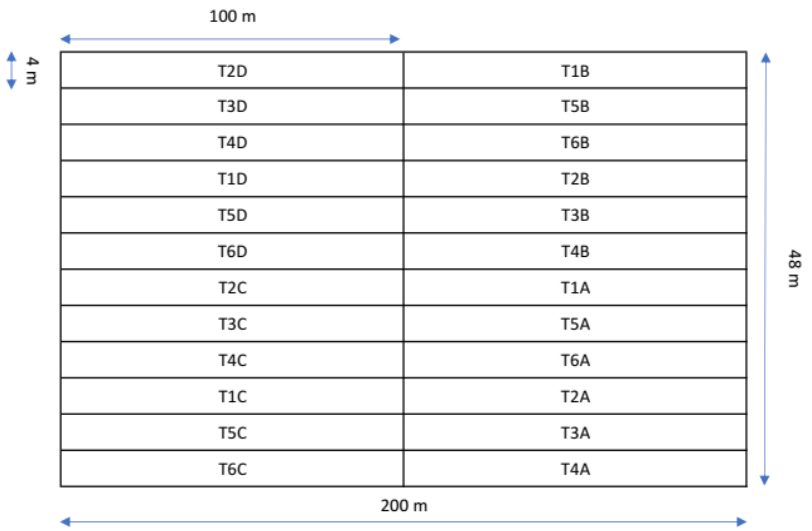

Fig. 2. Distribution of the trial plots across the field. To identify each repetition of the same configuration, each one was named by adding a letter to the trial number (e.g., T1A for the first repetition, T1B for the second, etc.)

The implement working depth (δ) was maintained at 150 mm for every tested condition. This parameter was achieved by adjusting the height of the packer roller of the harrow. The packer roller does influence the soil aggregate dimension, and it is challenging to separate his work from that of the harrow. However, since the characteristics and the position of the packer roller were maintained constant during all the trials, its contribution to the soil fragmentations could be considered constant. So, the comparison between the different trials remains consistent.

2.5. Field operation data analysis

The acquired signals were interpolated at 10 Hz with a cubic spline in Matlab® (Natick, MA, USA) to standardise all of the signals to the same sampling rate and remove high-frequency disturbances.

The maximum implement–soil impact speed (V_{is}) was calculated by;

$$V_{is} = n_{ph}\frac{2\pi}{60}R_{ph} + V_t \tag{3}$$

while the tractor's actual engine power (P_e) was calculated by;

$$P_e = M_r\frac{M_e - M_f}{100}n_e\frac{2\pi}{60} \tag{4}$$

and the torque applied to the power harrow rotors was calculated using;.

$$M_{ph} = \frac{M_{PTO}}{\tau_{ph}} \tag{5}$$

The efficiency of the power harrow transmission was not considered as it did not change among the tested configurations.

The total power absorbed by the power harrow (P_{ph}) was calculated using Eq. (6) as the sum of the power used to tow the implement (P_D) and the power used to run the power harrow rotors through the PTO (P_{PTO}) was calculated by Eqs. (7) and (8);

$$P_D = D\ V_t \tag{6}$$

$$P_{PTO} = M_{ph}\ n_{ph}\ \frac{2\pi}{60} \tag{7}$$

$$P_{ph} = P_D + P_{PTO} \tag{8}$$

221 The power delivery efficiency (η) was calculated by;

$$\eta = \frac{P_{ph}}{P_e} \tag{9}$$

222 The field capacity (F_c) and the fuel consumption per hectare (f_{ha}) in each pass were also
223 calculated by;

$$F_c = b\ V_t \tag{10}$$

$$f_{ha} = \frac{\dot{f}}{F_c} \tag{11}$$

224 The energy required to process 1 m^3 of tilled soil (E) was calculated using;

$$E = \frac{P_{ph}}{V_t\ b\ \delta} \tag{12}$$

225 The passes were separated from the headland turns (Fig. 3a) observing the rate of change of
226 P_{ph}, calculated with the signal differentiation (Fig. 3b).

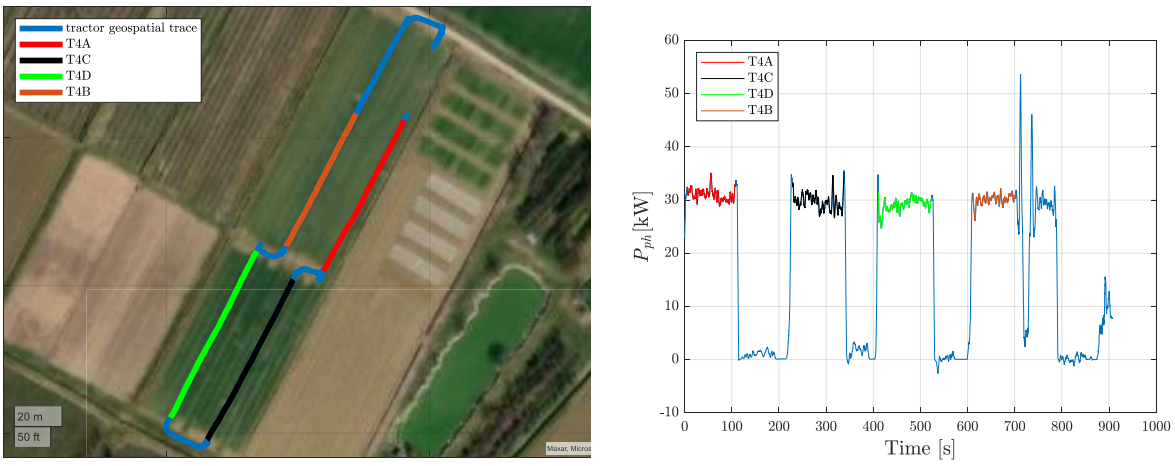

a b

227 **Fig. 3.** (a) Spatial position of the tractor during the tests; (b) Passes and headland turns, shown
228 as the rate of change of the power absorbed by the power harrow (P_{ph}) signal.

After harrowing, following ASTM D2488 (2009a) procedures, about 8 kg of dry tilled soil were collected at the depth range of 0 – 150 mm from each parcel to determine the aggregate size distribution. Soil samples were sieved following the ASTM D6913/D6913M-17 (2021) procedures, using five BS ISO 3310-2 (2013) sieves with nominal hole sizes (d_i) of 2, 4, 8, 16, and 31.5 mm (Fig. 4).

Fig. 4. From left to right and top to bottom: Sieves with diameters d_i of 31.5, 16, 8, 4, and 2 mm and the residual collector.

The percentage of soil mass retained ($W_{i,j}^{r\%}$) in the i^{th} sieve collected in the j^{th} parcel was calculated by;

$$W_{i,j}^{r\%} = \frac{W_{i,j}^{r}}{\sum_{i=1}^{n_s} W_{i,j}^{r}} \cdot 100 \tag{13}$$

where $W_{i,j}^{r}$ is the mass of soil collected in the j^{th} parcel retained by the i^{th} sieve and n_s is the number of sieves (5).

The MWD and the GMD (Van Bavel, 1950) of the aggregates were calculated for each parcel by;

$$MWD = \sum_{i=1}^{n_s} d_i \, W_{i,j}^{r\%} \tag{14}$$

$$GMD = \exp\left[\sum_{i=1}^{n_s} \ln(d_i) \, W_{i,j}^{r\%}\right] \tag{15}$$

To obtain an agronomic evaluation of the granulometry, the soil texture index k_t, derived from Natsis et al. (1999) and adapted to be consistent with the dimensions of the sieves used in this study, was determined for each configuration using ;

$$k_t = \frac{W_{j,0-8}}{W_{j,>8}} \tag{16}$$

where $W_{j,0-8}$ is the mass of soil with clods between 0 and 8 mm, while $W_{j,>8}$ is the mass of soil with clods over 8 mm. The index k_t indicates the quality of the seedbed. A threshold value of 8 mm was chosen after considering the available literature about optimal seedbed conditions in terms of soil aggregate sizes for the seed germination of various crops (Adam & Erbach, 1992; Braunack & Dexter, 1989; Munkholm, 2002; Tapela & Colvin, 2002).

To evaluate the soil skeleton proportion in each parcel, the index k_s was calculated by;

$$k_s = \frac{W_{j,>32}}{W_j} \tag{17}$$

where $W_{j,32}$ is the mass of soil retained by the 31.5 mm sieve and W_j is the total mass of soil collected in the j^{th} parcel. So, the trials that produced better-quality seedbeds could be identified as those with higher k_t values and lower k_s values. The mean values of V_t, V_{is}, C, D, P_e, P_D, P_{PTO}, P_{ph}, f_{ha}, MWD, GMD, k_s and k_s acquired during the passes were calculated and denoted with the overbar and the superscript p for each parameter.

Subsequently, to highlight significant correlations between the collected soil and energetic indicators, a Spearman's correlation matrix was performed using the built-in *corr* function in

Matlab (Mathworks inc., Natick, MA, USA). The parameters that showed correlation indices over 0.6 were identified and possible regression curves were investigated, as shown in the example in Fig. 5.

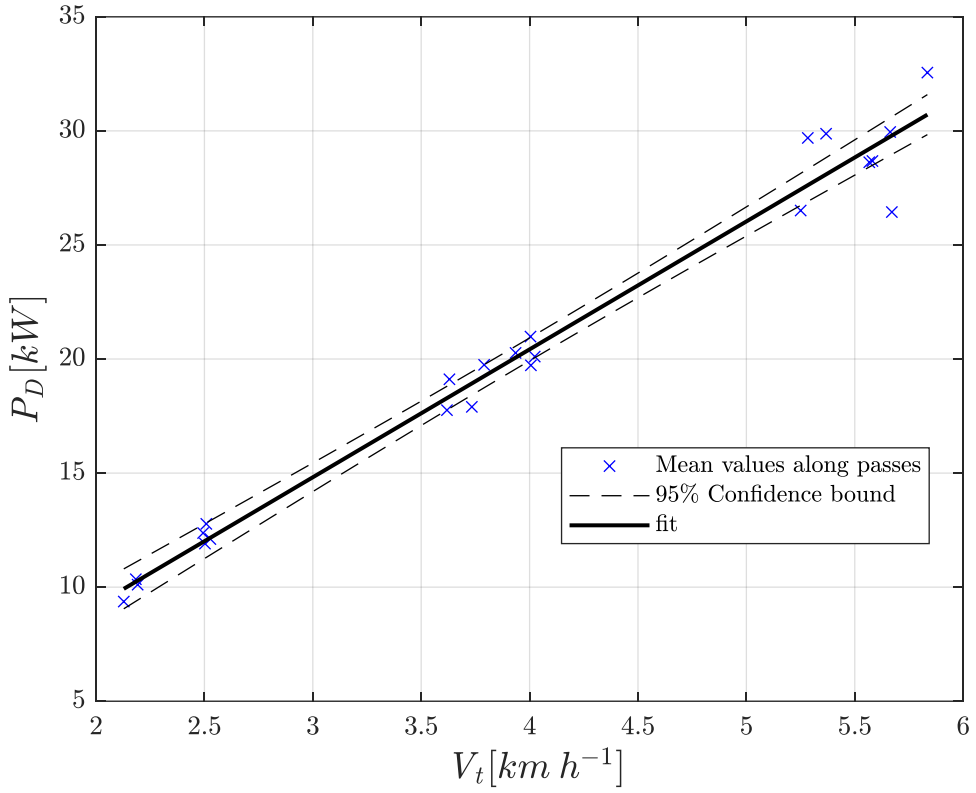

Fig. 5. Linear regression of drought power($\bar{P}_D^p$) as a function of tractor speed ($\bar{V}_t^p$). The details of this regression are reported in Appendix A, Table A2.

Finally, to obtain a global overview of the results, the mean values and standard deviations of the mean values along passes were calculated for each configuration. These means were denoted with only the overbar. That is, V_t represents the raw signal, $\bar{V}_t^p$ represents the mean value during one pass, and $\bar{V}_t$ represents the mean value of the $\bar{V}_t^p$ obtained from each repetition. The resulting values were compared to each other with several one-way ANOVA tests to evaluate any significant differences.

3. Results

This section describes and interprets the experimental results.

3.1. Methodology validation and operational mean values

The actual values of $\bar{V}_t$, $\bar{n}_{ph}$, and $\bar{\lambda}$ during the trials are shown in Table 4.

Table 4. Measured $\bar{\lambda}$ values from each test compared with the theoretical target values (standard deviation in brackets).

Parameters	T1	T2	T3	T4	T5	T6
Target V_t [km h^{-1}]	6.6	6.6	4.0	2.5	3.8	2.1
$\bar{V}_t$ [km h^{-1}]	5.5 (0.17)	5.5 (0.27)	4.0 (0.04)	2.5 (0.01)	3.7 (0.08)	2.2 (0.03)
Target n_{ph} [rev min^{-1}]	256	398	256	184	340	440
$\bar{n}_{ph}$ [rev min^{-1}]	222 (5.95)	345 (15.6)	251 (2.43)	184 (1.11)	352 (8.02)	488 (8.60)
Target λ	1.46	2.27	2.41	2.77	3.37	7.90
$\bar{\lambda}$	1.52 (5.51 10^{-3})	2.35 (9.21 10^{-3})	2.37 (1.17 10^{-3})	2.77 (5.08 10^{-3})	3.59 (1.18 10^{-2})	8.49 (1.45 10^{-2})
$\bar{\lambda}$ per cent difference from target λ [%]	3.7	3.3	-1.7	-0.27	6.4	7.5

The only tests showing a significant difference from the target V_t were T1 and T2. These demanded a P_e close to the maximum tractor power (Table 4), making maintaining the desired configuration difficult. However, the $\bar{n}_{ph}$ values were lower than intended for the same reason, so the $\bar{\lambda}$ in these tests was not very far from the target value. As Table 4 shows, the actual value of $\bar{\lambda}$ in all the tests did not exceed a 7.5% difference from the target value, so the tests were considered consistent with the designed methodology.

In Table 5, the mean values of the other measured parameters in the passes for each configuration are reported.

Table 5. Tractor and power harrow mean values of the measured parameters among the passes (standard deviation values in brackets)

Parameters	T1	T2	T3	T4	T5	T6
$\bar{V}_{is}$ [km h^{-1}]	13.9 (0.4)	18.5 (0.9)	13.5 (0.1)	9.4 (0.1)	16.9 (0.4)	20.6 (0.4)
$\bar{D}$ [kN]	19.1 (0.8)	18.8 (1.6)	18.3 (0.5)	17.6 (0.6)	18.2 (0.8)	16.5 (0.6)
$\bar{M}_{PTO}$ [Nm]	426 (28)	527 (19)	379 (19)	311(15)	375 (22)	379 (36)
$\bar{M}_{ph}$[Nm]	1,253 (80)	994 (36)	1,116(57)	917 (43)	1,101 (64)	861 (81)
$\bar{P}_e$ [kW]	109.6 (0.3)	109.1 (0.8)	98.3 (1.3)	63.9 (2.5)	106.4 (3.1)	93.7 (3.5)
$\bar{P}_{PTO}$ [kW]	29.1 (1)	35.8 (1.7)	29.3 (1.3)	17.7 (0.9)	40.5 (2.2)	44 (3.4)
$\bar{P}_D$ [kW]	29.2 (0.7)	28.8 (2.9)	20.3 (0.5)	12.3 (0.4)	18.6 (1)	9.9 (0.5)
$\bar{P}_{ph}$ [kW]	58.4 (1.4)	64.7 (3)	49.6 (1.2)	30 (0.8)	59.2 (2.8)	53.9 (2.9)
$\bar{\eta}$ [-]	0.53 (0.01)	0.59 (0.02)	0.5 (0.01)	0.47 (0.01)	0.56 (0.01)	0.58 (0.05)
$\bar{f}$ [L h^{-1}]	31.3 (0.2)	31.2 (0.4)	30 (0.2)	18.8 (0.6)	30.9 (0.9)	28.6 (1.3)
$\bar{f}_{ha}$ [L ha^{-1}]	18.6 (0.1)	18.9 (0.5)	24.9 (0.2)	25 (0.7)	27.6 (0.3)	43.6 (2)
$\bar{E}$ [kJ m^{-3}]	84.6 (4.5)	93.6 (2.1)	99.4 (3.2)	95.6 (2)	128.2 (6.1)	199.2 (13.8)
$\overline{MWD}$ [mm]	18.7 (2.1)	14.6 (0.4)	17.4 (0.7)	17.7 (1.1)	17.2 (2.5)	15.2 (0.9)
$\overline{GMD}$ [mm]	12.7 (2.2)	9.1 (0.2)	11.4 (0.9)	11.6 (1.2)	11.6 (2.7)	9.8 (0.6)
$\bar{k}_t$[-]	0.6 (0.19)	1.05 (0.03)	0.68 (0.11)	0.69 (0.14)	0.7 (0.32)	0.89 (0.08)
$\bar{k}_s$[-]	0.45 (0.08)	0.29 (0.03)	0.39 (0.02)	0.41 (0.04)	0.38 (0.08)	0.3 (0.05)

The analysis of the standard deviations shows that the registered values were generally low; the highest variations were found in D and M_{ph} and, therefore, P_D and P_{PTO}, which are related through Eqs. (11) and (12), respectively. This is mainly due to the natural variability of the soil characteristics between the parcels.

3.2. Tractor and power harrow performance parameter correlations

The correlation matrix obtained with the values along the passes is shown in Fig. 6.

	V_t	n_{ph}	V_{is}	λ	D	M_{PTO}	M_{ph}	P_D	P_{PTO}	P_{ph}	P_e	η	$\dot{f}$	f_{ha}	E	MWD	GMD	k_t	k_s
V_t	1.00																		
n_{ph}	-0.09	1.00																	
V_{is}	0.07	0.92	1.00																
λ	-0.89	0.44	0.23	1.00															
D	0.61	-0.24	-0.19	-0.61	1.00														
M_{PTO}	0.69	0.32	0.51	-0.55	0.33	1.00													
M_{ph}	0.59	-0.23	-0.21	-0.55	0.54	0.41	1.00												
P_D	0.95	-0.14	0.03	-0.89	0.79	0.67	0.60	1.00											
P_{PTO}	-0.14	0.91	0.85	0.46	-0.21	0.42	-0.04	-0.15	1.00										
P_{ph}	0.61	0.52	0.66	-0.33	0.40	0.84	0.33	0.61	0.61	1.00									
P_e	0.85	0.15	0.34	-0.68	0.56	0.78	0.68	0.84	0.23	0.81	1.00								
η	0.25	0.75	0.84	0.02	0.12	0.74	0.03	0.27	0.82	0.87	0.51	1.00							
$\dot{f}$	0.83	0.28	0.39	-0.58	0.52	0.73	0.62	0.79	0.31	0.82	0.93	0.53	1.00						
f_{ha}	-0.84	0.43	0.20	0.94	-0.53	-0.50	-0.33	-0.83	0.47	-0.33	-0.58	-0.04	-0.50	1.00					
E	-0.71	0.61	0.36	0.89	-0.38	-0.32	-0.34	-0.68	0.62	-0.14	-0.48	0.19	-0.37	0.92	1.00				
MWD	0.07	-0.52	-0.58	-0.18	0.17	-0.43	0.36	0.07	-0.54	-0.39	-0.04	-0.60	0.01	-0.12	-0.29	1.00			
GMD	0.03	-0.45	-0.51	-0.13	0.11	-0.41	0.32	0.03	-0.48	-0.40	-0.07	-0.56	-0.02	-0.07	-0.22	0.97	1.00		
k_t	0.01	0.43	0.49	0.08	-0.16	0.43	-0.33	-0.02	0.44	0.37	0.06	0.52	0.03	0.00	0.16	-0.92	-0.96	1.00	
k_s	0.12	-0.63	-0.66	-0.27	0.17	-0.34	0.44	0.11	-0.58	-0.37	0.01	-0.63	0.04	-0.18	-0.37	0.95	0.89	-0.83	1.00

Fig. 6. Results of the Spearman's correlation matrix. High correlations are highlighted in dark grey.

Figure 7 shows that D is directly proportional to V_t in the experimental speed interval and the regression of D with respect to V_t is reported in Fig. 7.

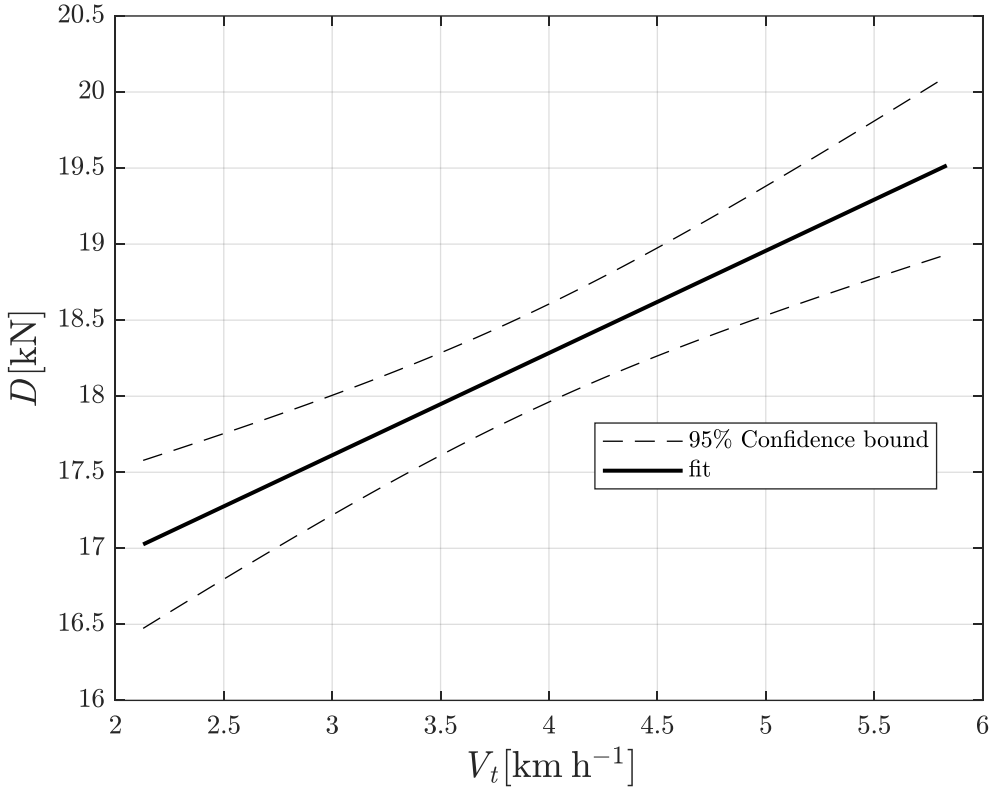

307

308 **Fig. 7** Linear regression of the drought (D) as a function of the tractor speed (V_t). The details
309 of this regression are reported in Appendix A, Table A1

310 This linear correlation differs from that observed when using typical passive tillage tools,
311 such as mouldboard ploughs and subsoilers, where a quadratic correlation was noticed (ASAE,
312 2015). The relatively low R^2 value obtained for this regression (0.6) is due to the variability of
313 the soil characteristics, which caused a certain variability in the D values. Similar results have
314 been reported in studies on other tillage tools (Godwin, 2007; Perumpral et al., 1983). Because
315 D is linearly dependent on V_t, P_D should exhibit a quadratic dependence on V_t (Eq. 6). However,
316 the slope of D–V_t has a low gradient. The highest registered value of $\overline{D}$ is only 16% higher than
317 the lowest one, while the highest value of $\overline{V_t}$ is more than double the lowest one. Therefore, a
318 linear correlation was found between P_D and V_t as was already showed in Fig. 5.

319

320

This dependence of both D and P_D on V_t results in the recorded maximum values of around 19 kN and 29 kW, respectively, at 5.5 km h^{-1}.

A correlation coefficient of 0.91 was found between P_{PTO} and n_{ph}. The results of this regression are presented in Fig. 8. This result is due to the relationship shown in Eq. (7); no significant correlation was found between n_{ph} and M_{ph}, as shown by the low coefficient (-0.23) obtained in the correlation matrix.

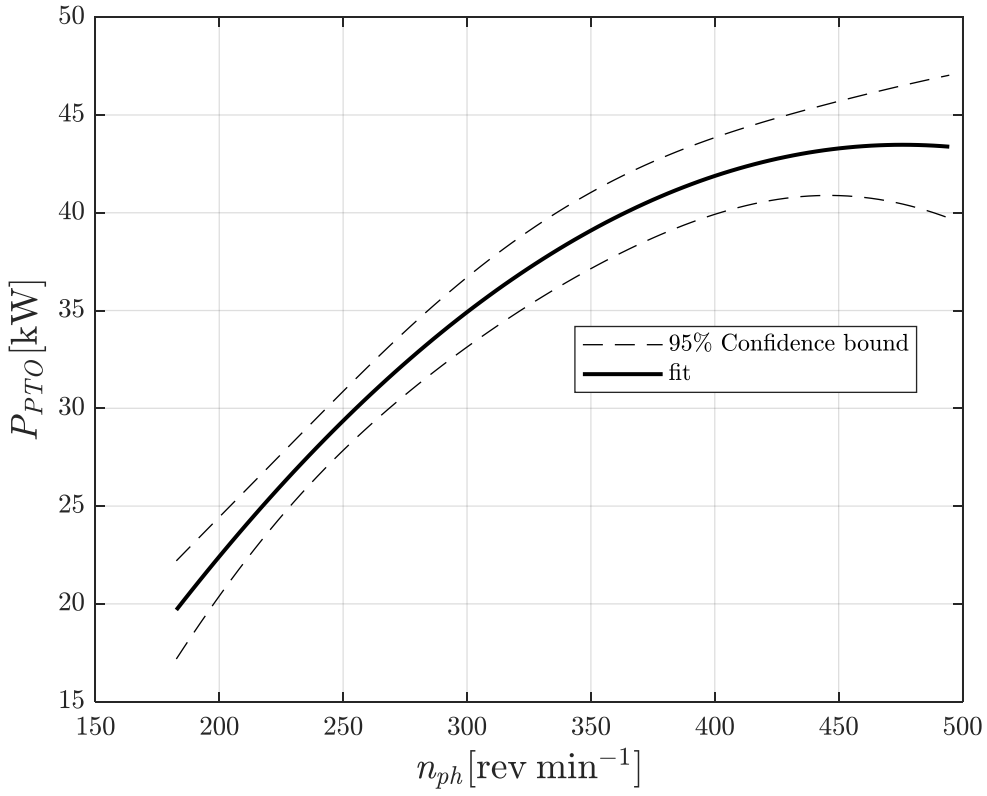

Fig. 8. Polynomial regression curve of the power used to run the power harrow rotors (P_{PTO}) as a function of rotational speed of the power harrow rotors (n_{ph}). The details of this regression are reported in Appendix A, Table A3.

There is a monotonic correlation between increasing n_{ph} and P_{PTO}, which agrees with the existing literature (Akbolat & Ekinci, 2008; Celik & Altikat, 2022). In particular, the curve shows a steep increase of P_{PTO} at low values of n_{ph}, which then flattens, reaching maximum values of around 44 kW at 488 rpm.

The relationship between M_{ph} and V_t that was observed in similar work by Balsari (2021) and Khsetri (2021) was partially confirmed by our study. The correlation index was 0.59, confirming that $\bar{M}_{ph}$ increases with increasing $\bar{V}_t$, except in the T2 trials, which did not follow this trend as their values were lower than expected. This is mainly because the T2 trial configuration was performed with a $\bar{P}_e$ that was close to the maximum tractor power, which limited the maximum reachable value of $\bar{P}_{PTO}$, and, consequently the maximum reachable $\bar{M}_{ph}$ value. Thus, a significant regression curve between M_{ph} and V_t could not be obtained.

As expected, the correlation matrix shows a high correlation between P_e, P_{ph}, and $\dot{f}$ because these parameters depend on each other. However, Fig. 9 shows that η increases with increasing P_{ph}.

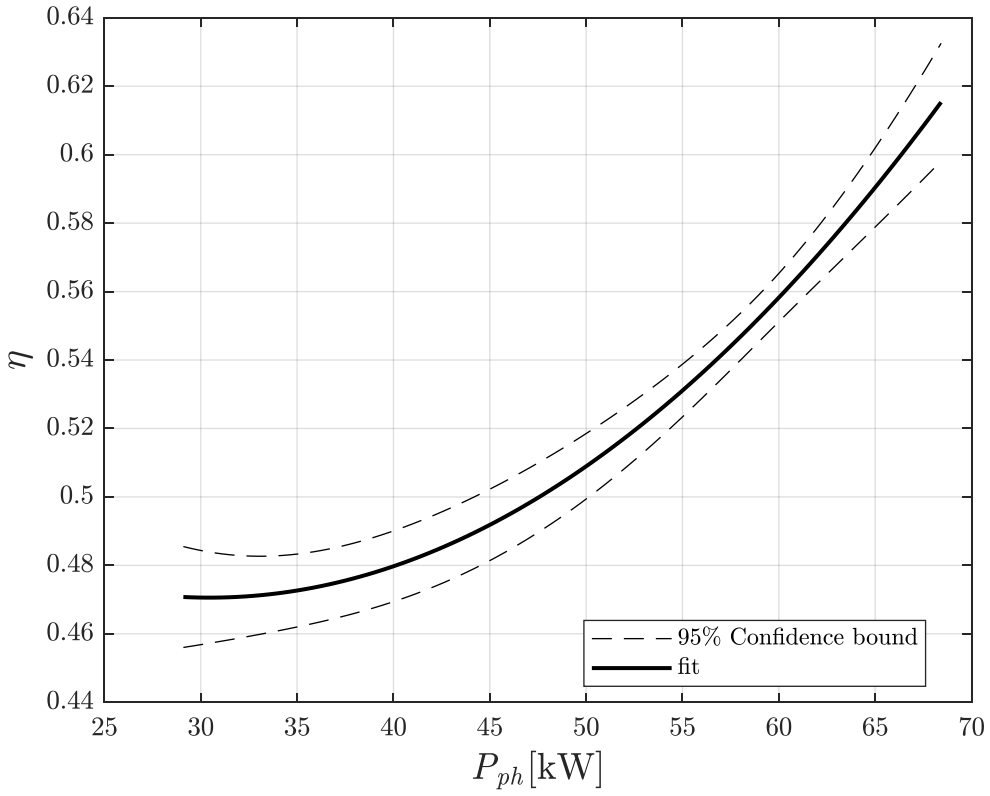

Fig. 9. Polynomial regression curve of the power delivery efficiency (η) as a function of the power absorbed by the power harrow (P_{ph}). The details of this regression are reported in Appendix A, Table A4.

In particular, η shows a remarkable efficiency improvement of around 25% from the lowest to the highest values of P_{ph}. This is because low values of P_{ph} correspond to low values of P_e, and at low values of P_e, the percentage of power that is not used to run the power harrow (i.e. power required by tractor auxiliaries, power losses due to motion resistance, etc.) decreases with P_e, increasing the percentage of P_{ph} as well (Mattetti et al., 2020; Saetti et al., 2021). This leads to an increase of η with P_{ph}, the opposite behaviour from that observed when using passive implements. The increased speed leads to an increase in draught, thus increasing slippage, which lowers the global operational efficiency. However, PTO-driven implements have much lower draught than passive implements, leading to lower slippage values and greater slippage efficiency. The η measured in this study was similar to that observed on a disk plough in Shafaei et al. (2021), probably due to the flow of power through the PTO via engine-to-PTO transmission.

Moreover, the correlation matrix shows that η and V_{is} are highly correlated (0.84). Fig. 10 shows that η increases linearly with V_{is}, so tillage operations performed with high V_t and n_{ph} are highly efficient.

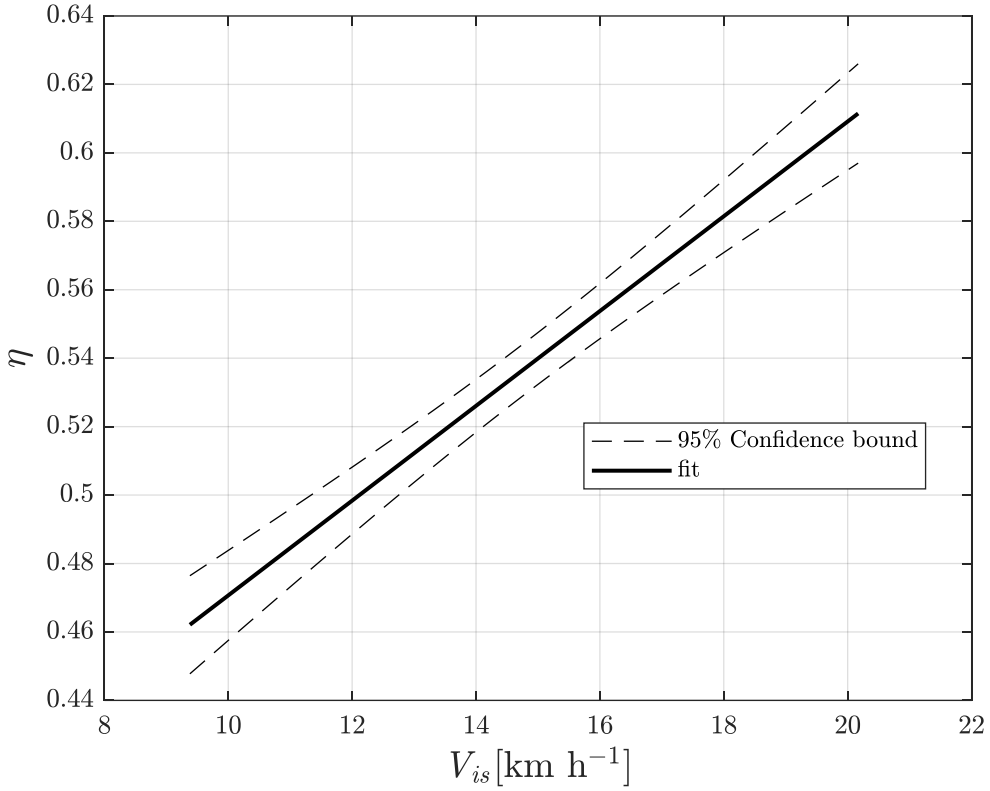

Fig. 10. Linear regression of power delivery efficiency (η) as a function of the implement-soil impact speed(V_{is}). The details of this regression are reported in Appendix A, Table A5.

This is mainly because P_{ph} and V_{is} are directly correlated, as shown by the correlation matrix index (0.61), so the behaviour observed between η and P_{ph} was similarly present between η and V_{is}. Performing the harrowing operation at high values of n_{ph} and, in particular, at high values of V_t leads to high P_{ph} values.

A strong linear correlation was found between E, f_{ha}, and λ (Fig. 11).

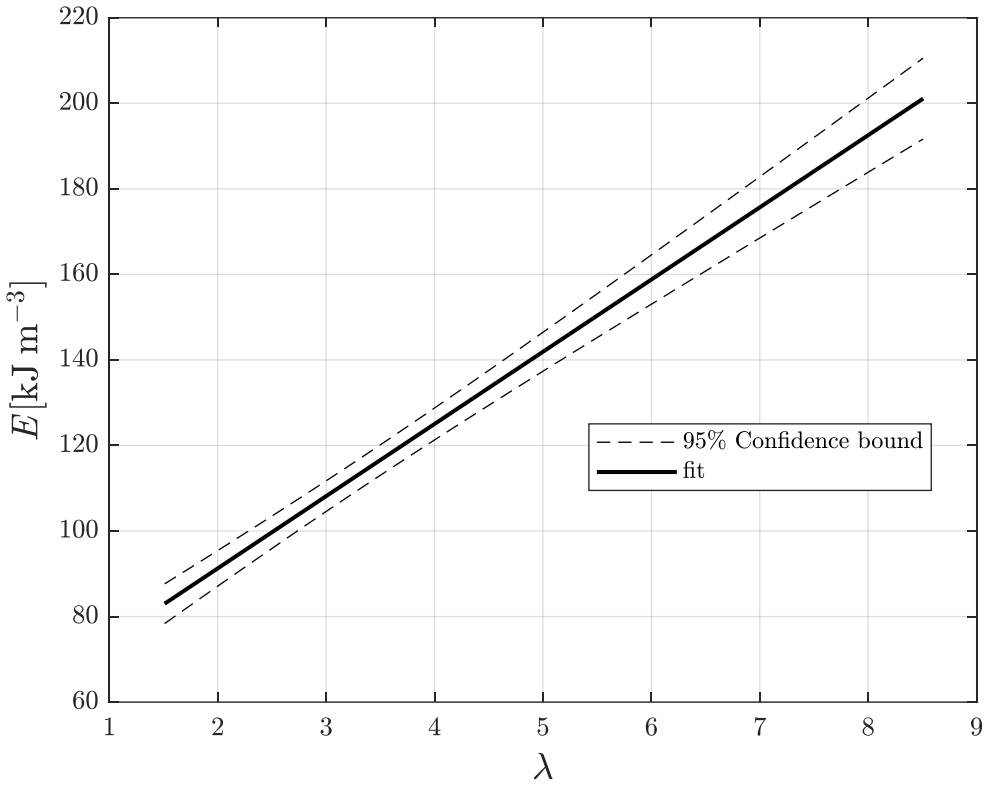

Fig. 11. Linear regression of the energy required to process 1 m^3 of tilled soil (E) as a function of the velocity ratio (λ). The details of this regression are reported in Appendix A, Table A6.

The value of E increases linearly with λ starting from values around 85 kJ m^{-3} at 1.52 to 200 kJ m^{-3} at 8.49. Results with similar magnitudes and behaviour were obtained by Balsari (2021) and Daraghmeh (2019) on silt loam and clay loam soil, respectively. As λ is the ratio of the peripheral speed of the tine rotors and the advancing speed of the tractor, high values of this parameter indicate greater distances travelled by the tines and, consequently, more energy required to till a defined volume of soil. The behaviour of f_{ha} matches that of E, so it has not been shown. These two parameters are bonded from an energetic point of view; with increased energy required to till the soil, more fuel will be used.

Unexpectedly, the values of λ and E do not appear to be directly correlated to the soil aggregate dimensions MWD and GMD; the lowest mean values were obtained in T2: 14.6 mm and 9.1 mm for MWD and GMD, respectively. However, both MWD and GMD showed a monotonic decrease with increasing V_{is}, as reported in Fig. 12.

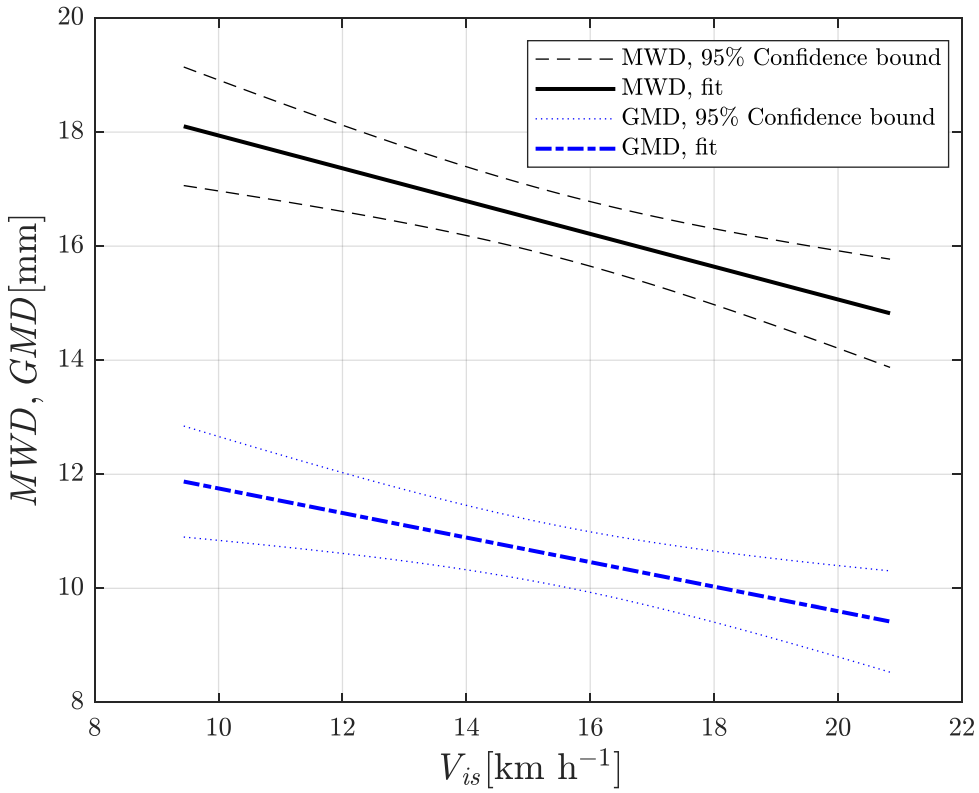

Fig. 12. Linear regression of MWD (black) and GMD (red) as functions of the implement-soil impact speed (V_{is}). The details of these regressions are reported in Appendix A, Tables A7 and A8 for MWD and GMD, respectively.

This result can be explained by the increasing soil disaggregation with the relative speed between the soil and rotors as the inertial force increases the overall soil reaction force (McKyes, 1985; Salokhe et al., 1994; Upadhyay & Raheman, 2020b). Both regressions showed relatively low R^2 values (0.57 for MWD-V_{is} and 0.46 for GMD-V_{is}) due to the variability of soil engineering properties, including soil bulk density, soil cohesion, internal friction angle, soil moisture content, and soil shear strength (Abo Al-kheer, Eid, et al., 2011; Abo Al-kheer, El-Hami, et al., 2011), the variability of the operational conditions, including tool working

speed, and the fact that manually sieving the soil implies a certain variability. Additionally, higher variability was observed from the configurations with working points far from the ideal $\bar{\lambda}$ value of 2.5, such as T1 and T5. Although T6 had a $\bar{\lambda}$ value 3.4 times higher than the ideal value for the implement used in this study, it did not show the high variability observed in T1 and T5. This is because $\bar{V}_t$ was very low in T6, so despite the implement being worked far from the ideal $\bar{\lambda}$ value, the soil was worked for enough time to make it dimensionally homogeneous. The values of k_t and k_s are highly correlated to MWD and GMD, as shown in the correlation matrix in Fig. 7. As expected, observing the values of $\bar{k}_t$ presented in Table 5 reveals that they decrease with increasing MWD and GMD, while $\bar{k}_s$ exhibits the opposite behaviour. The lowest value of $\bar{k}_t$, 0.60, was registered in T1, followed by values that ranged from 0.68 to 0.70 for T3, T4, and T5 and values over 0.89 for T2 and T6. T2 registered the maximum value of 1.05, which is an optimal value for the seeding process (Natsis et al., 1999). The values of $\bar{k}_s$ are inversely proportional to $\bar{k}_t$; the trials that registered the lowest values were T2 (0.29) and T6 (0.30). In T1, the value of $\bar{k}_s$ was 0.45, meaning that only 55% of the soil passed through the 31.5 mm sieve, revealing that the tilled soil still presented big clods, a condition that is unsuitable for seeding. In summary, from an agronomic point of view, the best configurations were T2 and T6 because they showed high $\bar{k}_t$ values and low $\bar{k}_s$ values.

3.3. Operational feasibility correlated with soil aggregate dimensions and energetic demand

Considering the results obtained in Ssection 3.2, V_{is} strongly influences the soil aggregate dimensions and operational efficiency. However, from a practical perspective, this parameter can be difficult to achieve because it is not immediately available to the operator who is performing the harrowing operation. To solve this problem, Nataraj et al.(2021) developed a wheel slip and velocity ratio warning system for rotary tillage tools, however these kind of

systems are not very widespread. Typically, the operator selects the V_t and n_{ph} values to adopt based on their previous experiences with the same contour conditions or by performing some preliminary passes to find acceptable working conditions. In particular, the choice of V_t is of paramount importance from an economic point of view as it is directly related to F_c (Eq. 10), which defines the duration of the operation, and f_{ha}(Eq. 11), which defines its costs. However, adjustments made with the aforementioned methodologies are unlikely to find the optimum condition that is economically and environmentally sustainable while simultaneously ensuring an optimum level of soil fragmentation. So, the trials performed at the same $\bar{V}_t$ with different $\bar{n}_{ph}$ (and, consequently, different $\bar{\lambda}$ and $\bar{V}_{is}$) were grouped in Table 6 to highlight any significant differences in terms of their energetic and soil fragmentation indicators.

Table 6 Trial tertiles as functions of $\bar{V}_t$

Group	Tests	$\bar{V}_t$ [km h^{-1}]	$\Delta\bar{V}_t$ [km h^{-1}]	$\bar{n}_{ph}$ [rev min^{-1}]	$\bar{\lambda}$
Low speed (LS)	T4	2.5	0.3	184	2.77
	T6	2.2		488	8.49
Medium speed (MS)	T3	4.0	0.3	251	2.37
	T5	3.7		352	3.59
High speed (HS)	T1	5.5	0.0	222	1.52
	T2	5.5		345	2.35

The comparison between the $\overline{\text{MWD}}$, $\bar{E}$, $\bar{\dot{f}}$, and $\bar{f}_{ha}$ values are reported in the bar graphs shown in Fig. 13 for the LS, MS, and HS terciles. The GMD, k_t and k_s were excluded from the analysis to improve its readability as their behaviours were proportional to MWD, as shown in section 3.2. The detailed results of these one-way ANOVA tests are reported in Appendix B.

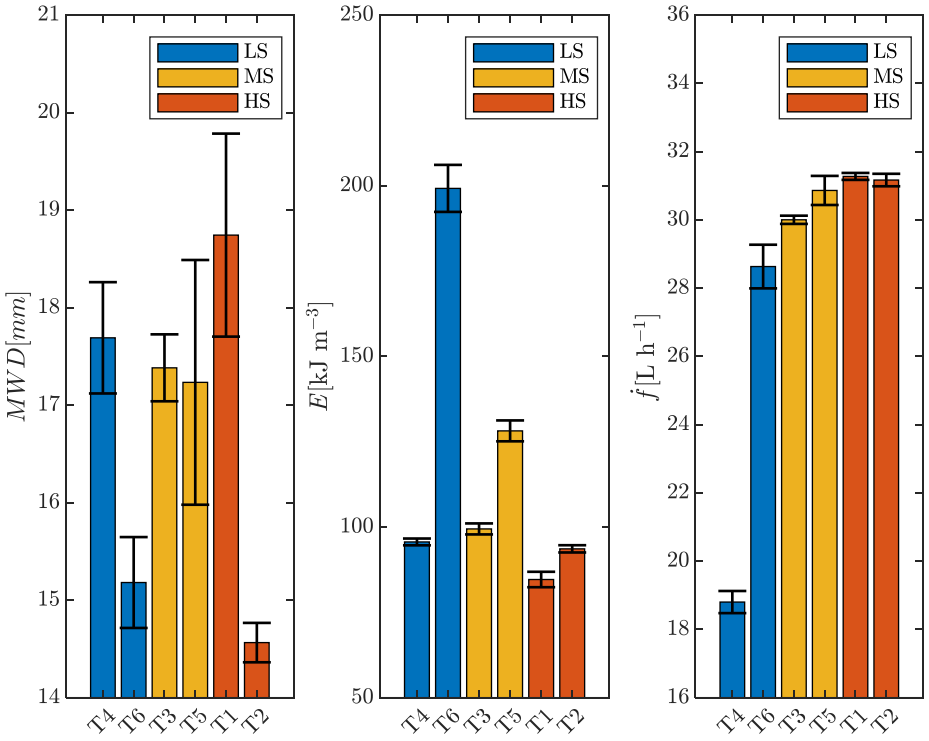

Fig. 13. $\overline{MWD}$, the energy required to process 1 m^3 of tilled soil ($\overline{E}$) and the fuel rate ($\bar{\dot{f}}$) values for the low speed (LS), medium speed (MS), and high speed (HS) terciles. The error bars represent the standard deviations. The details of the one-way ANOVA test results are reported in Appendix B, Tables B1 to B9.

As expected, at similar $\bar{V}_t$ values, the significant differences in n_{ph} between the configurations caused significant differences in the mean values between the pairs of configurations, confirmed by the results of the ANOVA test. In particular, the $\overline{\mathrm{MWD}}$ value of T4 is 16% higher than that of T6, while, the $\bar{E}$ value of T4 is 52% lower than that of T6. The $\bar{f}_{ha}$ value of 46.6 l ha^{-1} that was recorded in T6, which has an extremely high $\bar{\lambda}$ value, is economically and environmentally unsustainable, despite the suitability of the obtained soil particle size for further agricultural operations.

In the MS group, no significant difference was found in terms of $\overline{\mathrm{MWD}}$, so the obtained soil particle size was similar in the two configurations. However, T3 requires 22% less energy to till the same volume of soil due to its lower $\bar{\lambda}$ value. This leads to a mean value of 25.0 L ha^{-1},

459 which is 2.6 L ha^{-1} lower than the value registered in T5. Thus, there are no economic or
460 environmental reasons to prefer the T5 configuration over T3.

461 The ANOVA test performed on the HS group showed a significant difference in terms of
462 $\overline{\mathrm{MWD}}$ and $\bar{E}$ between the two configurations due to their different $\bar{\lambda}$ values. The mean MWD
463 value in T1 is 28% higher than that in T2, while $\bar{E}$ in T1 was 10% lower than in T2. However,
464 both configurations showed almost identical mean $\bar{f}_{ha}$ values, with 18.6 L ha^{-1} for T1 and 18.9
465 L ha^{-1} for T2. This leads to the conclusion that T2 was the overall best configuration,
466 simultaneously ensuring the best soil disaggregation and a very low value of $\bar{f}_{ha}$.

467 ## 4. Conclusions

468 Many farmers conduct tillage operations as routine practice, unaware of the effects of these
469 practices on the quality of the seedbed and their operational efficiency. Farmers must know
470 how to adequately set up their machinery; otherwise, all the efforts of manufacturers and
471 researchers are of limited utility. This paper presents the results of an extensive in-field
472 experimental campaign in which several indicators of a tractor–power harrow system and the
473 seedbed quality were monitored under different working conditions. The tests consisted of six
474 different field operation configurations performed to achieve varying λ, from a theoretical
475 minimum value of 1.46 to a theoretical maximum value of 7.90. A Spearman's correlation
476 matrix revealed several significant correlations between the investigated indicators. An
477 interesting result is that a significant operational efficiency improvement, around 25%, was
478 obtained as the power absorbed by the power harrow and the implement–soil impact speed
479 moved from lower to higher values. Moreover, the fuel consumption per hectare was found to
480 linearly increase with the velocity ratio, with a difference in the mean values of the two most
481 extreme tested configurations of 25.0 L ha^{-1}. That said, the value of λ was not correlated to the

soil fragmentation indicators. These were instead correlated with the implement–soil impact speed. Indeed, high implement–soil impact speeds reduce the soil aggregate size.

In summary, the optimum conditions to ensure a high-quality seedbed are obtained with high implement–soil impact speeds and the lowest possible λ values to reduce the fuel consumption per hectare. In practice, extremely low λ values are unreachable at high implement–soil impact speeds as extremely high tractor speeds would become necessary and these are limited by the tractor–power harrow system and soil characteristics. Moreover, extremely low λ values should be avoided because the power harrow would then work almost as a passive implement, creating the potential to overstress the rotor bearings. The results presented in this paper will be useful for the development of new variable-rate tillage implements, a topic of high interest in recent years (Mohammadi et al., 2022). The ongoing challenge is to achieve more homogenous aggregate sizes over fields with heterogeneous soil properties during seedbed preparation (Riegler-Nurscher et al., 2020).

Acknowledgements

This project was supported by PRIN (Research Projects of Significant National Interest), notification 2015, ‘Optimization of operating machinery through analysis of the mission profile for more efficient agriculture’, grant number 2015KTY5NW.

References

Abo Al-kheer, A., Eid, M., Aoues, Y., El-Hami, A., Kharmanda, M. G., & Mouazen, A. M. (2011). Theoretical analysis of the spatial variability in tillage forces for fatigue analysis of tillage machines. *Journal of Terramechanics*, *48*(4), 285–295. https://doi.org/10.1016/j.jterra.2011.05.002

Abo Al-kheer, A., El-Hami, A., Kharmanda, M. G., & Mouazen, A. M. (2011). Reliability-based design for soil tillage machines. *Journal of Terramechanics*, *48*(1), 57–64. https://doi.org/10.1016/j.jterra.2010.06.001

Adam, K. M., & Erbach, D. C. (1992). Secondary tillage tool effect on soil aggregation. *Transactions of the ASAE (USA)*. https://doi.org/10.13031/2013.28796

Akbolat, D., & Ekinci, K. (2008). Rotary tiller velocity effects on the distribution of wheat (Triticum aestivum) residue in the soil profile. *New Zealand Journal of Crop and Horticultural Science*, *36*(4), 247–252. https://doi.org/10.1080/01140670809510241

ASAE. (2015). *D497.7 Agricultural Machinery Management Data*.

ASTM. (2009a). *D2488—Practice for Description and Identification of Soils (Visual-Manual Procedure)*. ASTM International.

ASTM. (2009b). *Standard Test Methods for Laboratory Determination of Density (Unit Weight) of Soil Specimens*.

ASTM. (2010). *Test Methods for Liquid Limit, Plastic Limit, and Plasticity Index of Soils.ASTM International*.

ASTM. (2021). *ASTM D6913/D6913M-17—Standard Test Methods for Particle-Size Distribution (Gradation) of Soils Using Sieve Analysis*.

Balázs, B., Kelemen, E., Centofanti, T., Vasconcelos, M. W., & Iannetta, P. P. M. (2021). Integrated policy analysis to identify transformation paths to more sustainable legume-based food and feed value-chains in Europe. *Agroecology and Sustainable Food Systems*, *45*(6), 931–953. https://doi.org/10.1080/21683565.2021.1884165

Balsari, P., Biglia, A., Comba, L., Sacco, D., Eloi Alcatrão, L., Varani, M., Mattetti, M., Barge, P., Tortia, C., Manzone, M., Gay, P., & Ricauda Aimonino, D. (2021). Performance analysis of a tractor—Power harrow system under different working conditions. *Biosystems Engineering*, *202*, 28–41. https://doi.org/10.1016/j.biosystemseng.2020.11.009

Beckman, J., Ivanic, M., Jelliffe, J., Baquedano, F. G., & Scott, S. (2020). *Economic and Food Security Impacts of Agricultural Input Reduction Under the European Union Green Deal's Farm to Fork and Biodiversity Strategies* (EB-30; Economic Brief, p. 59). http://www.ers.usda.gov/publications/pub-details/?pubid=99740

Borin, M., Menini, C., & Sartori, L. (1997). Effects of tillage systems on energy and carbon balance in north-eastern Italy. *Soil and Tillage Research*, *40*(3), 209–226. https://doi.org/10.1016/S0167-1987(96)01057-4

Braunack, M. V., & Dexter, A. R. (1989). Soil aggregation in the seedbed: A review. I. Properties of aggregates and beds of aggregates. *Soil and Tillage Research*, *14*(3), 259–279. https://doi.org/10.1016/0167-1987(89)90013-5

Bronick, C. J., & Lal, R. (2005). Soil structure and management: A review. *Geoderma*, *124*(1), 3–22. https://doi.org/10.1016/j.geoderma.2004.03.005

BS ISO. (2013). *BS ISO 3310-2:2013 Test sieves—Technical requirements and testing*.

Celik, A., & Altikat, S. (2022). The effect of power harrow on the wheat residue cover and residue incorporation into the tilled soil layer. *Soil and Tillage Research*, *215*, 105202. https://doi.org/10.1016/j.still.2021.105202

Chen, Y., Cavers, C., Tessier, S., Monero, F., & Lobb, D. (2005). Short-term tillage effects on soil cone index and plant development in a poorly drained, heavy clay soil. *Soil and Tillage Research*, *82*(2), 161–171. https://doi.org/10.1016/j.still.2004.06.006

Choudhary, S., Upadhyay, G., Patel, B., Naresh, & Jain, M. (2021). Energy Requirements and Tillage Performance Under Different Active Tillage Treatments in Sandy Loam Soil. *Journal of Biosystems Engineering*, *46*(4), 353–364. https://doi.org/10.1007/s42853-021-00112-y

Daraghmeh, O. A., Petersen, C. T., Munkholm, L. J., Znova, L., Obour, P. B., Nielsen, S. K., & Green, O. (2019). Impact of tillage intensity on clay loam soil structure. *Soil Use and Management*, *35*(3), 388–399. https://doi.org/10.1111/sum.12501

Dedousis, A. P., & Bartzanas, T. (2010). *Soil engineering.* Springer Science & Business Media.

Dexter, A. R., & Bird, N. R. A. (2000). Methods for predicting the optimum and the range of soil water contents for tillage based on the water retention curve. *Soil and Tillage Research*, *57*(4), 203–212. Scopus. https://doi.org/10.1016/S0167-1987(00)00154-9

Garnett, T., Appleby, M. C., Balmford, A., Bateman, I. J., Benton, T. G., Bloomer, P., Burlingame, B., Dawkins, M., Dolan, L., Fraser, D., Herrero, M., Hoffmann, I., Smith, P., Thornton, P. K., Toulmin, C., Vermeulen, S. J., & Godfray, H. C. J. (2013). Sustainable Intensification in Agriculture: Premises and Policies. *Science*. https://doi.org/10.1126/science.1234485

Godwin, R. J. (2007). A review of the effect of implement geometry on soil failure and implement forces. *Soil and Tillage Research*, *97*(2), 331–340. https://doi.org/10.1016/j.still.2006.06.010

Godwin, R. J., O'Dogherty, M. J., Saunders, C., & Balafoutis, A. T. (2007). A force prediction model for mouldboard ploughs incorporating the effects of soil characteristic properties, plough geometric factors and ploughing speed. *Biosystems Engineering*, *97*(1), 117–129. https://doi.org/10.1016/j.biosystemseng.2007.02.001

Hann, M. J., & Giessibl, J. (1998). Force Measurements on Driven Discs. *Journal of Agricultural Engineering Research*, *69*(2), 149–157. https://doi.org/10.1006/jaer.1997.0241

Heege, H. J. (A c. Di). (2013). *Precision in Crop Farming: Site Specific Concepts and Sensing Methods: Applications and Results*. Springer Netherlands. https://doi.org/10.1007/978-94-007-6760-7

Kshetri, S., Steward, B. L., & Tekeste, M. Z. (2021). Modeling Soil Forces on a Rotary Tine Tool in Artificial Soil. *Transactions of the ASABE*, *64*(5), 1693–1704. https://doi.org/10.13031/trans.14336

Köppen, W. (1936). Das geographische system der climate. *Handbuch der klimatologie. I, Teil, C*.

Mattetti, M., Varani, M., Maraldi, M., Paolini, F., Fiorati, S., & Molari, G. (2020). Tractive performance of Trelleborg PneuTrac tyres. *Journal of Agricultural Engineering*, *51*(2), Art. 2. https://doi.org/10.4081/jae.2020.1031

Mattetti, M., Varani, M., Molari, G., & Morelli, F. (2017). Influence of the speed on soil-pressure over a plough. *Biosystems Engineering*, *156*, 136–147. https://doi.org/10.1016/j.biosystemseng.2017.01.009

McKyes, E. (1985). Soil cutting and tillage. *Soil Cutting and Tillage.*

590 Mohammadi, F., Maleki, M., & Khodaei, J. (2022). Control of variable rate system of a rotary
591 tiller based on real-time measurement of soil surface roughness. *Soil and Tillage Research*,
592 *215*, 105216. https://doi.org/10.1016/j.still.2021.105216

593 Munkholm, L. J. (2002). *Soil Fragmentation and Friability. Effects of Soil Water and Soil*
594 *Management* [Doctoral dissertation, Danish Institute of Agricultural Sciences]. Danish
595 Institute of Agricultural Sciences.

596 Nataraj, E., Sarkar, P., Raheman, H., & Upadhyay, G. (2021). Embedded digital display and
597 warning system of velocity ratio and wheel slip for tractor operated active tillage
598 implements. *Journal of Terramechanics*, *97*, 35–43.
599 https://doi.org/10.1016/j.jterra.2021.06.003

600 Natsis, A., Papadakis, G., & Pitsilis, J. (1999). The Influence of Soil Type, Soil Water and Share
601 Sharpness of a Mouldboard Plough on Energy Consumption, Rate of Work and Tillage
602 Quality. *Journal of Agricultural Engineering Research*, *72*(2), 171–176.
603 https://doi.org/10.1006/jaer.1998.0360

604 Nunes, M. R., Denardin, J. E., Pauletto, E. A., Faganello, A., & Pinto, L. F. S. (2015). Effect of
605 soil chiseling on soil structure and root growth for a clayey soil under no-tillage. *Geoderma*,
606 *259–260*, 149–155. https://doi.org/10.1016/j.geoderma.2015.06.003

607 Perumpral, J., Grisso, R., & Desai, C. (1983). A Soil-Tool Model Based on Limit Equilibrium
608 Analysis. *Transactions of the ASAE*, *26*, 0991–0995. https://doi.org/10.13031/2013.34062

609 Raparelli, T., Eula, G., Ivanov, A., & Pepe, G. (2020). Kinematic analysis of rotary harrows.
610 *Journal of Agricultural Engineering*, *51*(1), Art. 1. https://doi.org/10.4081/jae.2019.976

611 Riegler-Nurscher, P., Moitzi, G., Prankl, J., Huber, J., Karner, J., Wagentristl, H., & Vincze,
612 M. (2020). Machine vision for soil roughness measurement and control of tillage machines
613 during seedbed preparation. *Soil and Tillage Research*, *196*, 104351.
614 https://doi.org/10.1016/j.still.2019.104351

615 Saetti, M., Mattetti, M., Varani, M., Lenzini, N., & Molari, G. (2021). On the power demands
616 of accessories on an agricultural tractor. *Biosystems Engineering*, *206*, 109–122.
617 https://doi.org/10.1016/j.biosystemseng.2021.03.015

618 Salokhe, V. M., Islam, M. S., Gupta, C. P., & Hoki, M. (1994). Field testing of a PTO powered
619 disk tiller. *Journal of Terramechanics*, *31*(2), 139–152. https://doi.org/10.1016/0022-
620 4898(94)90011-6

621 Scarlett, A. J. (2001). Integrated control of agricultural tractors and implements: A review of
622 potential opportunities relating to cultivation and crop establishment machinery. *Computers*
623 *and Electronics in Agriculture*, *30*(1), 167–191. https://doi.org/10.1016/S0168-
624 1699(00)00163-0

625 Shafaei, S. M., Loghavi, M., & Kamgar, S. (2021). Analytical Description of Power Delivery
626 Efficiency of Front Wheel Assist Tractor in Tillage Works. *Journal of Biosystems*
627 *Engineering*, *46*(3), 236–253. https://doi.org/10.1007/s42853-021-00103-z

628 Shinners, K. J., Wilkes, J. M., & England, T. D. (1993). Performance Characteristics of a
629 Tillage Machine with Active-Passive Components. *Journal of Agricultural Engineering*
630 *Research*, *55*(4), 277–297. https://doi.org/10.1006/jaer.1993.1050

631 Sukcharoenvipharat, W., & Usaborisut, P. (2018). EFFICIENCY TESTS OF ROTARY
632 TILLER AND POWER HARROW. *International Journal of Advances in Science*
633 *Engineering and Technology*, *6*(1). https://doi.org/10.5281/zenodo.1132557

634 Tapela, M., & Colvin, T. S. (2002). Quantifying seedbed condition using soil physical
635 properties. *Soil and Tillage Research*, *64*(3), 203–210. https://doi.org/10.1016/S0167-
636 1987(01)00267-7

637 Upadhyay, G., & Raheman, H. (2020a). Effect of velocity ratio on performance characteristics
638 of an active-passive combination tillage implement. *Biosystems Engineering*, *191*, 1–12.
639 https://doi.org/10.1016/j.biosystemseng.2019.12.010

640 Upadhyay, G., & Raheman, H. (2020b). Comparative assessment of energy requirement and
641 tillage effectiveness of combined (active-passive) and conventional offset disc harrows.
642 *Biosystems Engineering*, *198*, 266–279.
643 https://doi.org/10.1016/j.biosystemseng.2020.08.014

644 USDA. (1984). *Usual Planting and Harvesting Dates for U.S. Field Crops*. U.S. Department
645 of Agriculture, Statistical Reporting Service.

646 USDA. (1987). *Soil Mechanichs Level I*.

647 Van Bavel, C. H. M. (1950). Mean weight-diameter of soil aggregates as a statistical index of
648 aggregation. *Proceedings. Soil Science Society of America*, *1949*, *14*, 20–23.

649 van Bavel, C. H. M. (1950). Mean Weight-Diameter of Soil Aggregates as a Statistical Index
650 of Aggregation. *Soil Science Society of America Journal*, *14*(C), 20–23.
651 https://doi.org/10.2136/sssaj1950.036159950014000C0005x

652 Watts, C. W., Dexter, A. R., & Longstaff, D. J. (1996). An assessment of the vulnerability of
653 soil structure to destabilisation during tillage. Part II. Field trials. *Soil and Tillage Research*,
654 *37*(2), 175–190. https://doi.org/10.1016/0167-1987(95)01001-7

655 Weill, A. N., McKyes, E., & Kimpe, C. R. D. (1989). Effect of tillage reduction and fertilizer
656 on soil macro- and microaggregation. *Canadian Journal of Soil Science*, *69*(3), 489–500.
657 https://doi.org/10.4141/cjss89-051

Appendix A

In this appendix are reported the details of the regression curves presented in section 3.2 of this paper

Table A1 Goodness of fit of D as a function of V_t

Parameter	Value
Model equation	$D = p1\ V_t + p2$
Fitting Method	Linear least squares
p1 (95% confidence bounds)	0.67 (0.42, 0.93)
p2 (95% confidence bounds)	15.60 (14.56, 16.63)
SSE	10.43
R^2	0.61
RMSE	0.72
Number of outliers	1

Table A2 Goodness of fit of P_D as a function of V_t

Parameter	Value
Model equation	$P_D = p1\ V_t + p2$
Fitting Method	Linear least squares
p1 (95% confidence bounds)	5.61 (5.22, 5.99)
p2 (95% confidence bounds)	-2.00 (-3.63, -0.38)
SSE	28.0
R^2	0.98
RMSE	1.15
Number of outliers	0

Table A3 Goodness of fit of P_{PTO} as a function of n_{ph}

Parameter	Value
Model equation	$P_{PTO} = p1\ {n_{ph}}^2 + p2\ n_{ph} + p3$
Fitting Method	Linear least squares
p1 (95% confidence bounds)	$-2.77\ 10^{-4}$ ($-4.00\ 10^{-4}$, $-1.00\ 10^{-4}$)
p2 (95% confidence bounds)	0.26 (0.17, 0.35)
p3 (95% confidence bounds)	-19.18 (-33.10, -5.25)
SSE	168.46
R^2	0.90
RMSE	2.90
Number of outliers	0

666 **Table A4** Goodness of fit of η as a function of P_{ph}

Parameter	Value
Model equation	$\eta = p1\ {P_{ph}}^2 + p2\ P_{ph} + p3$
Fitting Method	Linear least squares
p1 (95% confidence bounds)	$1.00\ 10^{-5}$ ($1.00\ 10^{-4}$, $1.00\ 10^{-4}$)
p2 (95% confidence bounds)	$-6.12\ 10^{-3}$ ($-1.05\ 10^{-2}$, $-1.70\ 10^{-3}$)
p3 (95% confidence bounds)	0.56 (0.47, 0.66)
SSE	$3.30\ 10^{-3}$
R^2	0.92
RMSE	$1.33\ 10^{-2}$
Number of outliers	1

667 **Table A5** Goodness of fit of η as a function of V_{is}

Parameter	Value
Model equation	$\eta = p1\ V_{\mathrm{is}t} + p2$
Fitting Method	Linear least squares
p1 (95% confidence bounds)	$1.38\ 10^{-2}$ ($1.16\ 10^{-2}$, $1.61\ 10^{-2}$)
p2 (95% confidence bounds)	$3.32\ 10^{-1}$ ($2.98\ 10^{-1}$, $3.67\ 10^{-1}$)
SSE	$5.19\ 10^{3}$
R^2	0.90
RMSE	$1.65\ 10^{2}$
Number of outliers	2

668 **Table A6** Goodness of fit of E as a function of λ

Parameter	Value
Model equation	$E = p1\ \lambda + p2$
Fitting Method	Linear least squares
p1 (95% confidence bounds)	16.88 (15.20, 18.56)
p2 (95% confidence bounds)	57.52(50.93, 64.10
SSE	$1.40\ 10^{3}$
R^2	0.95
RMSE	8.17
Number of outliers	0

669

670 **Table A7** Goodness of fit of *MWD* as a function of V_{is}

Parameter	Value
Model equation	$MWD = p1\ V_{\mathrm{ist}} + p2$
Fitting Method	Linear least squares
p1 (95% confidence bounds)	$-2.88\ 10^{-1}$ ($-4.31\ 10^{-1}$, $-1.44\ 10^{-1}$)
p2 (95% confidence bounds)	20.81 (18.52, 23.12)
SSE	15.4
R^2	0.57
RMSE	1.05
Number of outliers	2

671 **Table A8** Goodness of fit of *GMD* as a function of V_{is}

Parameter	Value
Model equation	$GMD = p1\ V_{\mathrm{ist}} + p2$
Fitting Method	Linear least squares
p1 (95% confidence bounds)	$-2.15\ 10^{-1}$ ($-3.50\ 10^{-1}$, $-8.07\ 10^{-2}$)
p2 (95% confidence bounds)	13.90 (11.75, 16.05)
SSE	13.5
R^2	0.46
RMSE	$9.82\ 10^{-1}$
Number of outliers	2

672

673

Appendix B

In this appendix are reported the details of the one way ANOVA tests presented in section 3.3 of this paper

Table B1 One way ANOVA test results for the *MWD* values between T4 and T6

Source	SS	df	MS	F	p>F
Groups	9.44	1	9.44	8.70	0.042
Error	4.34	4	1.09	-	-
Total	13.79	5	-	-	-

Table B2 One way ANOVA test results for the E values between T4 and T6

Source	SS	df	MS	F	p>F
Groups	21457.84	1	21457.85	328.60	$1.81\ 10^{-6}$
Error	391.80	6	65.30	-	-
Total	21849.65	7	-	-	-

Table B3 One way ANOVA test results for the $\dot{f}$ values between T4 and T6

Source	SS	df	MS	F	p>F
Groups	193.26	1	193.26	255.81	$3.79\ 10^{-6}$
Error	4.53	6	0.76	-	-
Total	197.79	7	-	-	-

Table B4 One way ANOVA test results for the *MWD* values between T3 and T5

Source	SS	df	MS	F	p>F
Groups	0.033	1	0.033	0.0098	0.92
Error	13.54	4	3.38	-	-
Total	13.57	5	-	-	-

Table B5 One way ANOVA test results for the E values between T3 and T5

Source	SS	df	MS	F	p>F
Groups	1650.36	1	1650.36	68.97	$1.7\ 10^{-4}$
Error	143.57	6	23.93	-	-
Total	1793.94	7	-	-	-

684 **Table B6** One way ANOVA test results for the $\dot{f}$ values between T3 and T5

Source	SS	df	MS	F	p>F
Groups	1.48	1	1.48	3.77	0.10
Error	2.35	6	0.39	-	-
Total	3.83	7	-	-	-

685 **Table B7** One way ANOVA test results for the *MWD* values between T1 and T2

Source	SS	df	MS	F	p>F
Groups	26.19	1	26.19	11.65	0.027
Error	8.99	4	2.25	-	-
Total	35.18	5	-	-	-

686 **Table B8** One way ANOVA test results for the *E* values between T1 and T2

Source	SS	df	MS	F	p>F
Groups	161.33	1	161.33	12.92	0.011
Error	74.90	6	12.48	-	-
Total	236.23	7	-	-	-

687 **Table B9** One way ANOVA test results for the $\dot{f}$ values between T1 and T2

Source	SS	df	MS	F	p>F
Groups	0.022	1	0.022	0.26	0.63
Error	0.52	6	0.087	-	-
Total	0.55	7	-	-	-

688

689

690